A Control Strategy for Salient-Pole Permanent Magnet Axial-Gap Self-Bearing Motors Considering Stator Inductance Variation

Ngo Kien Trung
Hanoi Industrial Textile Garment University, Hanoi, Vietnam
trungnk@hict.edu.vn

Duong Anh Tuan
Hanoi University of Industry, Hanoi, Vietnam
tuanda@haui.edu.vn

Tran Thuy Van
Hanoi University of Industry, Hanoi, Vietnam
vantt@haui.edu.vn

Vo Quang Vinh
Electric Power University, Hanoi, Vietnam
vinhvq@epu.edu.vn

Duong Quoc Tuan
Thai Nguyen University of Technology, Thai Nguyen, Vietnam
duongquoctuan-tdh@tnut.edu.vn (corresponding author)

Received: 21 November 2024 | Revised: 10 December 2024 | Accepted: 18 December 2024

 DOI: https://doi.org/10.48084/etasr.9676

ABSTRACT

Axial-Flux Self-Bearing Motors (AFBMs) are distinguished by considerable variations in inductance resulting from axial displacement. Conventional controllers are frequently engineered to accommodate a wide range of inductance changes. Nevertheless, this methodology is often suboptimal, particularly when inductance is not accurately determined. This paper puts forward a novel inductance approximation function for the stator, designed to minimize modeling errors. Furthermore, an advanced control strategy is presented, based on a sliding mode controller with online adaptive parameter tuning. The experimental results demonstrate the efficacy of the proposed control strategy, exhibiting enhanced performance, stability, and robustness across a range of operating conditions.

Keywords-self-bearing motor; Axial-Gap Self Bearing Motor (AGBM)

I. INTRODUCTION

Axial-flux motors have attracted considerable research attention due to their distinctive advantages. In comparison to radial-flux motors, axial-flux motors have been shown to generate higher torque, exhibit enhanced efficiency, and demonstrate increased power density. These characteristics render them particularly well-suited for applications that require optimization of space utilization [1]. In addition, in specialized applications, axial-flux motors can meet the requirements for precise axial positioning adjustments, categorizing them as Axial-Gap Self-Bearing Motors (AGBMs) [2-6]. The capability to control the axial position negates the need for mechanical restraints along the drive axis, offering an optimal solution for systems using active magnetic bearings [7]. Furthermore, the integration of active magnetic bearings with axial-flux self-levitating motors enables the attainment of comprehensive rotor control across all six degrees of freedom [8]. This integration offers distinct advantages, including a reduction in the overall size and an enhancement in the motor power density. Axial-flux motor configurations are typically classified into three primary categories: dual stator-single rotor, dual rotor-single stator, and multi-stator multi-rotor systems [3]. The stators, which are responsible for generating the magnetic field, typically employ

three-phase windings that generate a rotating magnetic field along the rotor's axial direction. The motor torque is generated by three primary factors:

- The interaction between the rotor flux and the stator current i_q.
- The reluctance torque, arising from the inductance disparity between the d-axis and q-axis of the motor.
- The flux differential across the air gap regions.

In the configuration of a dual-stator and a single-rotor system, incorporating a salient-pole rotor, the contributions of the reluctance torque and flux differential across the air gaps are negligible. Consequently, this configuration facilitates more efficient torque regulation. This study adopts this specific motor configuration to maximize the inherent advantages of the axial-flux motor design. Despite the structural differences, a common feature of these designs is the application of vector control techniques [8-12]. Similar to permanent magnet motors, the current and flux components in the motor are represented in the vector space, where the i_q current controls the torque and the i_d current regulates the flux linkage [13]. Field-Oriented Control (FOC) algorithms have been effective in torque regulation and speed control [11,12]. However, due to the nonlinear nature of the magnetic levitation, the control of the levitation force remains challenging. A common approach in motor control posits a stable operating position of the rotor, thereby enabling the linearization or simplification of system parameters. In such cases, traditional linear control strategies are widely employed [14,15]. Alternatively, nonlinear control strategies, proposed in [16-18], offer adaptability to parameter variations. However, these methods typically neglect the inductance variations along the z-axis of the motor, which can considerably influence the efficacy of the control, particularly within the current control loop. It is important to note that most control strategies assume that the motor starts at its equilibrium position, which complicates the accurate modeling of stator inductance. Authors in [8], indicate that the relationship between the stator inductance and air gap distance is primarily determined through experimental observations. As the air gap narrows, stator inductance increases sharply, and conversely, it decreases as the gap widens. This relationship can be modeled using exponential functions. To enhance the estimation accuracy of these inductance parameters, various algorithms have been examined [19, 20]. The present paper proposes a nonlinear backstepping control strategy that incorporates inductance variation along the z-axis. In addition, the motor model is presented, with an approximation of the stator inductance achieved through the use of an exponential function. This approximation of the stator inductance facilitates system operation across the entire positional range, rather than being constrained to a predefined equilibrium point. This aspect has not been adequately addressed in prior studies. The control architecture is presented including an outer-loop controller for speed and position and an inner-loop controller for current regulation. The controllers are then implemented on the hardware setup to validate the proposed approach. The experimental results obtained from this study confirm the effectiveness of the proposed control strategy, hence demonstrating enhanced stability and improved performance.

II. MATHEMATICAL MODEL OF THE MOTOR

The configuration of the motor can be seen in [8]. The system is composed of two stators and a rotor that uses permanent magnets. The axial position of the rotor is regulated by two magnetic bearings, either passive or active, thus effectively constraining the rotational angles along the x and y axes. In contrast, the rotor maintains flexible mobility along the z-axis. The mathematical model of the axial-flux self-levitating motor is derived from fundamental electromagnetic principles as described in [8]. The electrical model of the motor includes two sets of equations: one for stator 1 and another for stator 2, formulated in the d-q coordinate framework.

For stator 1:

$$\begin{cases} u_{sd1} = R_s i_{sd1} + L_{sd1}\frac{di_{sd1}}{dt} - \omega L_{sq1} i_{sq1} \\ u_{sq1} = R_s i_{sq1} + L_{sq1}\frac{di_{sq1}}{dt} + \omega\left(L_{sd1} i_{sd1} + \psi_p\right) \end{cases} \quad (1)$$

For stator 2:

$$\begin{cases} u_{sd2} = R_s i_{sd2} + L_{sd2}\frac{di_{sd2}}{dt} - \omega L_{sq2} i_{sq2} \\ u_{sq2} = R_s i_{sq2} + L_{sq2}\frac{di_{sq2}}{dt} + \omega\left(L_{sd2} i_{sd2} + \psi_p\right) \end{cases} \quad (2)$$

where, u_{sd1}, u_{sq1} are the d-axis and q-axis voltages for stator 1, respectively, while u_{sd2} and u_{sq2} are the corresponding voltages for stator 2, R_s is the stator resistance of the windings, i_{sd1}, i_{sq1}, i_{sd2}, and i_{sq2} are the d-axis and q-axis currents for each stator, ω is the angular velocity of the rotor, ψ_p is the magnetic flux produced by the permanent magnets on the rotor, and L_{sd1}, L_{sq1}, L_{sd2}, and L_{sq2} are the d-axis and q-axis inductances for stator 1 and stator 2, respectively. The AGBM exhibits two degrees of freedom: rotational motion along the z-axis and translational motion along the z-axis. Consequently, the dynamic behavior of the motor is described by (3) for rotational dynamics and (4) for translational motion:

$$\frac{3p}{2}\begin{bmatrix}\psi_p(i_{sq1}+i_{sq2}) + i_{sd1}i_{sq1}(L_{sd1}-L_{sq1}) \\ +i_{sd2}i_{sq2}(L_{sd2}-L_{sq2})\end{bmatrix} = m_m + \frac{J}{p}\frac{d\omega}{dt} \quad (3)$$

$$m\ddot{z} + F_L = k_1(i_{sd2} - i_{sd1}) + k_1(i_{sd2} + i_{sd1})z - k_2 z \quad (4)$$

where $k_1 = \frac{\mu_0^2 N^2}{g_0^2}\psi_p$, $k_2 = 2\frac{\mu_0}{S_p g_0}\psi_p^2$, z is the axial position of the motor, p is the number of the pole pairs of the motor, m is the mass of the rotor, and J is the moment of inertia of the motor. The structural parameters include N, the number of turns per pole in the stator, g_0, the nominal air gap distance, and μ_0, which is the permeability of free space. In the context of control design, inductance variations are typically disregarded. However, it is imperative to acknowledge that the stator inductance exerts a substantial influence on the electrical dynamics (1) and (2), as well as the torque of the motor (3). Fluctuations in inductance can lead to significant discrepancies in control, thereby compromising control accuracy. It is

noteworthy that the inductive components exhibit coupled variations, either increasing or decreasing in unison:

$$\begin{cases} i_{sd1} i_{sq1}(L_{sd1} - L_{sq1}) = 0 \\ i_{sd2} i_{sq2}(L_{sd2} - L_{sq2}) = 0 \end{cases} \quad (5)$$

Substituting (5) into the torque (3) results in:

$$\frac{3p}{2}\psi_p(i_{sq1} + i_{sq2}) = m_m + \frac{J}{p}\frac{d\omega}{dt} \quad (6)$$

As shown in (6), when the system is designed such that $L_{sd} = L_{sq}$, it can be observed that variations in inductance do not affect the dynamic equations. Consequently, the effects of inductance variations are primarily reflected within the current control mechanisms. One potential solution to this challenge involves the use of an approximation function, which allows for the rapid adaptation of the controller. The inductance of the coil has been shown to exhibit an inverse proportionality to the air gap distance. Furthermore, the experimental findings reported in [9] indicate that its variation can be effectively approximated by an exponential function. This function is employed to effectively represent the inductance variation along the z-axis. It is hypothesized that the motor's inductance follows an exponential function:

$$L(z) = L_0 e^{kz} \quad (7)$$

where k is the damping coefficient, with smaller values of k resulting in a reduced dependence of inductance on the rotor position, corresponding to a z-axis displacement that is much smaller than the air gap distance. Conversely, a larger k causes a more pronounced variation in the motor's inductance as the rotor position changes. The damping coefficient k and inductance L_0 are determined through experimental measurements conducted directly on the motor under investigation. Due to the opposite relative motion of the rotor with respect to the two stators, the inductance values of the stators vary in opposite directions:

$$\begin{cases} L_{sd1} = L_{sq1} = L_0 e^{kz} \\ L_{sd2} = L_{sq2} = L_0 e^{-kz} \end{cases} \quad (8)$$

Equation (8) enables a relatively accurate prediction of the motor's inductance, facilitating the rapid adjustment of the control signals to counteract a potential instability in controllers that do not account for this factor.

III. PROPOSED CONTROLLER

Conventional control strategies are not readily conducive to the straightforward and expeditious modification of controller parameters. Concurrently, the model parameters of the system under consideration in this paper exhibit rapid fluctuations. The incorporation of the system model into the control signals is expedited by a sliding mode controller [21-24]. This paper proposes a backstepping sliding mode controller design with two control loops: an outer loop consisting of speed and position controllers, and an inner loop serving as the current controller.

A. Speed Control

The speed and position control loops are not affected by the variations in stator inductance. Consequently, the controller design process is executed in a sequential manner. For the purpose of simplification, the variables are redefined and reformulated in a matrix form as: $\boldsymbol{I_{sq}} = [i_{sq1} \quad i_{sq2}]^T$, $b = \frac{3}{2} z_p \psi_p$. The expression describing the motion of the motor becomes:

$$\dot{\omega} = \frac{z_p}{J}\left(b\boldsymbol{I_{sq}} - m_m\right) \quad (9)$$

The Lyapunov function for the system (9) is chosen using:

$$V_\omega = \frac{1}{2}(\omega - \omega_r)^2 \quad (10)$$

where ω_r is the reference speed. By applying the derivative operator to both sides of (10) and substituting the result into (9), the following expression is obtained:

$$\dot{V_\omega} = (\omega - \omega_r)(\dot{\omega} - \dot{\omega}_r)$$
$$= (\omega - \omega_r)\left(\frac{z_p}{J}\left(\boldsymbol{B I_{sq}} - m_m\right) - \dot{\omega}_r\right) \quad (11)$$

By applying the LaSalle-Yoshizawa theorem, the control signal required for the system to reach the reference speed is obtained by:

$$\boldsymbol{I_{sq}} = b\left(m_m + \frac{J}{z_p}\left(\dot{\omega}_r - c_\omega(\omega - \omega_r)\right)\right) \quad (12)$$

With the current shown in (12), the system is stable. In fact, by substituting the control signal (12) into (11), the derivative of the Lyapunov function is obtained:

$$\dot{V_\omega} = -c_\omega(\omega - \omega_r)^2 < 0 \quad (13)$$

The derivative of the Lyapunov function in (13) is consistently negative, thereby fulfilling the conditions of Lyapunov's stability criterion. Consequently, the current I_{sq} in (12) is used for the design of the inner control loop, following the backstepping methodology.

B. Position Control

The bearing force acting on the motor rotor is generated by two currents, i_{sd1} and i_{sd2}, which flow in opposing directions. Rather than using i_{sd1} and i_{sd2} as independent control variables, it is proposed that an intermediate variable be applied, defined as the difference between the two currents:

$$\Delta I_d = i_{sd2} - i_{sd1} \quad (14)$$

The rotor position dynamics (4) is rewritten as:

$$K\Delta I_d - K_2 z - F_L = m_r \ddot{z} \quad (15)$$

where $K = k_1 + k_1 z$, and $K_2 = k_2 + 2k_1 i_{sd1}$. The translational dynamics equation of the motor includes a second-order derivative term. Consequently, the sliding surface is defined as a first-order inertia link:

$$S = \lambda z + \dot{z} \quad (16)$$

where λ is the inertia constant of the sliding surface. The sliding surface is characterized by two components: the position and the first derivative of the position (velocity) of the rotor along the axial direction. The sliding mode controller is designed to drive these two parameters to zero, under the condition that the chosen parameters fulfill the Hurwitz

stability criterion. The differentiation of both sides of (16) yields the following expression:

$$\dot{S} = \lambda\dot{z} + \ddot{z} = \lambda\dot{z} + \frac{1}{m_r}(K\Delta I_d - k_2 z - F_L) \quad (17)$$

The control signal of the sliding mode controller comprises two components. The first component drives the system's state variables towards the sliding surface, as described in (18), while the second component ensures the maintenance of the state variables on the sliding surface, as given in (19):

$$\Delta I_{dsw} = \frac{m_r}{K}(-\lambda\dot{z}) + \frac{1}{K}k_2 z + \frac{1}{K}F_L \quad (18)$$

$$\Delta I_{deq} = \frac{m_r}{K}\left(-c_z sign(S)\right) \quad (19)$$

Consequently, the final control signal is the combination of the two aforementioned components, which is expressed by:

$$\Delta I_d = \frac{m_r}{K}\left(-\lambda\dot{z} - c_z sign(S)\right) + \frac{1}{K}k_2 z + \frac{1}{K}F_L \quad (20)$$

The Lyapunov function for the system described in (20) is chosen as:

$$V_z = \frac{1}{2}S^2 \quad (21)$$

By differentiating both sides and substituting (17), the resulting expression is:

$$\dot{V}_z = S\dot{S} = S\left(\lambda\dot{z} + \frac{1}{m_r}(K\Delta I_d - k_2 z - F_L)\right) \quad (22)$$

Substituting the control signal (20) into (22) yields: $\dot{V}_z = -c_z S.sign(S) \leq 0$. Therefore, the employment of the control signal (20) enables the system to attain stability and drive the rotor position to its equilibrium state. In practical applications, an additional current i_{d0} is introduced to enhance system stability. The subsequent derivation provides the expression for determining the reference current for the inner current control loop:

$$\begin{cases} i_{sd1}^{ref} = i_{d0} + \Delta I_d \\ i_{sd2}^{ref} = i_{d0} - \Delta I_d \end{cases} \quad (23)$$

which will be used to compute the reference value for the current control loop.

C. Current control

In order to simplify the relationships between the current and voltage for the entire motor, the system of equations describing the motor's electrical relations is reformulated in a matrix form as:

$$\boldsymbol{L}_{dqz}\frac{d}{dt}\dot{\boldsymbol{I}}_{dq} = -\boldsymbol{C}\boldsymbol{I}_{dq} - \boldsymbol{D} + \boldsymbol{U}_{dq} \quad (24)$$

where $\boldsymbol{U}_{dq} = [u_{sd} \quad u_{sq}]^T$, $\boldsymbol{I}_{dq} = [i_{sd} \quad i_{sq}]^T$, $\boldsymbol{D} = [0 \quad \omega_s\psi_p]$, $\boldsymbol{L}_{dqz} = \begin{bmatrix} L_{sd}(z) & 0 \\ 0 & L_{sq}(z) \end{bmatrix}$, $\boldsymbol{C}_z = \begin{bmatrix} R_s & -\omega_s L_{sq}(z) \\ \omega_s L_{sd}(z) & R_s \end{bmatrix}$, and z is the dependence of inductance on the rotor position. Given the symmetric nature of the motor's structure, the controller design for the second stator follows a similar approach. The implementation of a sliding mode controller enables a seamless adjustment of the controller parameters, ensuring an effective modulation of system behavior. The error vector $\boldsymbol{e}_i = \boldsymbol{I} - \boldsymbol{I}_{dq}^{ref}$ is defined as the difference between the actual current values and the reference current values, where $\boldsymbol{I}_{dq}^{ref} = \begin{bmatrix} i_d^{ref} & i_q^{ref} \end{bmatrix}$ represents the desired dq current values.

Equation (24) can be reformulated by expressing the state variable in terms of the error vector as:

$$\dot{\boldsymbol{e}}_i = \boldsymbol{L}_{dq}{}^{-1}\left(\boldsymbol{U}_1 - \boldsymbol{C}_z\boldsymbol{e}_i - \boldsymbol{D}_1 - \boldsymbol{L}_{dq}\dot{\boldsymbol{I}}_{dq}^{ref} - \boldsymbol{C}_z\boldsymbol{I}_{dq}^{ref}\right) \quad (25)$$

In the absence of detailed information regarding the motor's inductance characteristics, the control signal selection will be based on the nominal inductance L_0 as a reference parameter. By applying the LaSalle-Yoshizawa theorem, the control signal is determined as:

$$\boldsymbol{U}_{dq} = \boldsymbol{C}_{z0}\dot{\boldsymbol{e}}_i + \boldsymbol{D} + \boldsymbol{L}_{dq0}\dot{\boldsymbol{I}}_{dq}^{ref} + \boldsymbol{C}_{z0}\boldsymbol{I}_{dq}^{ref} - \boldsymbol{K}_z\boldsymbol{e}_i \quad (26)$$

where $\boldsymbol{C}_{z0}$ and $\boldsymbol{L}_{dq0}$ are the $\boldsymbol{C}_z$ and $\boldsymbol{L}_{dqz}$ matrices at the position z=0, respectively, and $\boldsymbol{K}_z$ is the control gain matrix. To prove the stability of the system, the Lyapunov function is chosen as follows:

$$\boldsymbol{V}_1 = \frac{1}{2}\boldsymbol{e}_i^T\boldsymbol{e}_i \quad (27)$$

The derivative of both sides of (27) is taken, and by substituting the derivative from (25) and the control signal from (26), we obtain:

$$\dot{\boldsymbol{V}} = \boldsymbol{e}_i^T\dot{\boldsymbol{e}}_i = \boldsymbol{e}_i^T\boldsymbol{L}_1^{-1}(C_\Delta\boldsymbol{e}_i + L_\Delta\dot{\boldsymbol{I}}_{dq}^{ref} + C_\Delta\boldsymbol{I}_{dq}^{ref} - \boldsymbol{K}_z\boldsymbol{e}_i \quad (28)$$

where $\boldsymbol{C}_\Delta = \boldsymbol{C}_{z0} - \boldsymbol{C}_z = \omega_s L_0\begin{bmatrix} 0 & -(1-e^{kz}) \\ (1-e^{kz}) & 0 \end{bmatrix}$, $\boldsymbol{L}_\Delta = \boldsymbol{L}_0 - \boldsymbol{L}_1 = L_0(1-e^{kz})\begin{bmatrix} 1 & 0 \\ 0 & 1 \end{bmatrix}$, $\boldsymbol{L}_z = \frac{1}{L_0 e^{-kz}}\begin{bmatrix} 1 & 0 \\ 0 & 1 \end{bmatrix}$.

The matrices C and L represent the discrepancies between the actual model and the model utilized for the controller design. The substitution of the respective values of these matrices into (28) leads to:

$$\dot{\mathbf{V}}_1 = \mathbf{e}_i^T\dot{\mathbf{e}}_i = \mathbf{e}_i^T\left((e^{-kz}-1)\dot{\boldsymbol{I}}_r - \boldsymbol{L}^{-1}\boldsymbol{K}_z\mathbf{e}_i\right) = \underbrace{(e^{-kz}-1)\boldsymbol{e}_i^T\dot{\boldsymbol{I}}_r}_{\neq 0} - \underbrace{\boldsymbol{e}_i^T\boldsymbol{L}^{-1}\boldsymbol{K}_z\boldsymbol{e}_i}_{\leq 0} \quad (29)$$

Equation (29) demonstrates that a discrepancy between the model and the system has a substantial impact on the system, particularly during the startup phase when the displacement z is substantial and the reference current values undergo significant variations. The left-hand side of the expression, characterized by an undefined sign and magnitude, has the potential to induce instability in the system immediately from the initial point z_0. Consequently, the control signal in (26) is modified as:

$$\boldsymbol{U}_{dq} = \left(\boldsymbol{C}_0\boldsymbol{e}_i + \boldsymbol{D} + \boldsymbol{L}_z\dot{\boldsymbol{I}}_{dq}^{ref} + \boldsymbol{C}_0\boldsymbol{I}_{dq}^{ref} - K_1\boldsymbol{e}_i\right) \quad (30)$$

Using $L(z)$, determined in (8), the discrepancy between the model's inductance and the actual inductance is approximated as zero:

$$\dot{\boldsymbol{V}}_1 = \underbrace{\boldsymbol{e}_i\boldsymbol{L}^{-1}(\boldsymbol{L}_z - \boldsymbol{L})\dot{\boldsymbol{I}}_{dq}^{ref}}_{\approx 0} - \underbrace{\boldsymbol{e}_i^T\boldsymbol{L}^{-1}\boldsymbol{K}_z\boldsymbol{e}_i}_{\leq 0} \quad (31)$$

Given that the derivative of the Lyapunov function is less than or equal to zero, the system demonstrates asymptotic stability, ensuring that the deviation in the current will converge to zero over time. Finally, the current controller for the two stators is obtained and represented as:

$$\boldsymbol{U}_1 = \left(\boldsymbol{C}_1\boldsymbol{e}_{i1} + \boldsymbol{D}_1 + \boldsymbol{L}_{z1}\dot{\boldsymbol{I}}_{dq1}^{ref} + \boldsymbol{C}_1\boldsymbol{I}_{dq1}^{ref} - \boldsymbol{K}_{z1}\boldsymbol{e}_{i1}\right) \quad (32)$$

$$\boldsymbol{U}_2 = \left(\boldsymbol{C}_2\boldsymbol{e}_{i2} + \boldsymbol{D}_2 + \boldsymbol{L}_{z2}\dot{\boldsymbol{I}}_{dq2}^{ref} + \boldsymbol{C}_2\boldsymbol{I}_{dq2}^{ref} - \boldsymbol{K}_{z2}\boldsymbol{e}_{i2}\right) \quad (33)$$

In conclusion, the control signals presented in (32) and (33) comprise the core methodology for the design of the proposed controller, which incorporates the effects of the stator inductance variation along the z-axis. The structure of the proposed controller is depicted in Figure 1. In this configuration, the speed and position controllers function as the outer-loop controllers, while the current controllers for stator 1 and stator 2 serve as the inner-loop controllers. The position information obtained from the position sensor is fed back into the current controllers, allowing them to adapt to the inductance variations occurring during the control process, thus ensuring the stability of the system.

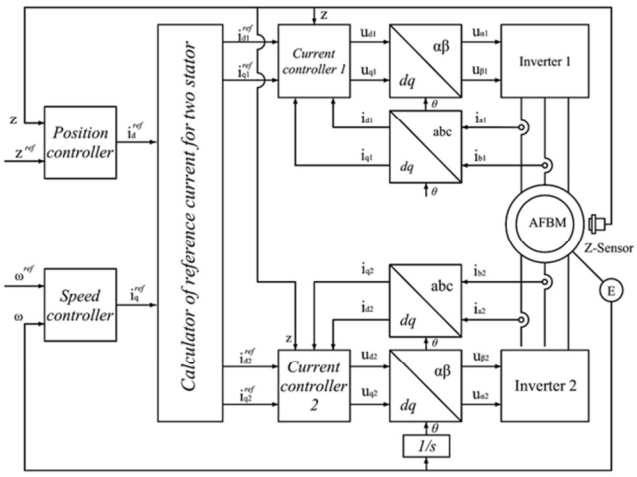

Fig. 1. Proposed control structure.

IV. EXPERIMENTAL RESULTS

A. AFBM Motor Model

In order to validate the proposed algorithm, a practical motor model was developed, as illustrated in Figure 2. The system consists of an AGBM motor featuring two stators and a single rotor. The stator's stationary component is engineered to move along a linear rail, while the rotor is fixed in position. Given the fixed position of the rotor, a distance sensor with a resolution of 2,000 μm is employed to measure the stator's position. The motor shaft is connected to an encoder with a resolution of 500 ppr to measure the rotor's speed and angular position. Additionally, a DC motor is employed to generate the load torque. The motor parameters are detailed in Table I. In order to reduce the possibility of overheating, which could result in motor failure, the converter is constrained to a maximum current of 5A. Consequently, the configuration of the controller parameters is structured in a manner that ensures that this restriction does not impose a substantial burden on the system's dynamic response characteristics. The inductance variation function (z) is constructed through direct measurements on the model, as displayed in Figure 3. Subsequently, using the fitting tool in MATLAB, the parameters in (8) are determined, with k_z = 0.23 and L_0 =8.2 mH. Substituting these values into the expression, the approximated function representing the relationship between inductance and the rotor's axial position z is:

$$L_{sd} = L_{sq} = 8.2 \times 10^{-3} e^{0.23z} (H) \quad (34)$$

Finally, the controllers are implemented on the MATLAB software and ControlDesk, with hardware integration utilizing the DS1104 system from dSPACE.

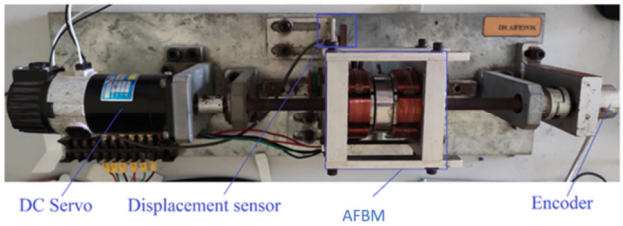

Fig. 2. Experimental setup of the AFBM.

TABLE I. PARAMETERS OF MOTOR

Parameter	Value	Unit
Stator resistance R_s	2.3	Ω
d-axis inductance at $z = 0$	8.2	mH
q-axis inductance at $z = 0$	8.2	mH
Rotor magnetic flux ψ_p	0.0126	Wb
Mass of rotor m	0.235	kg
Rotor moment of inertia J	8.2×10^{-6}	kgm^2
Pole pair p	1	

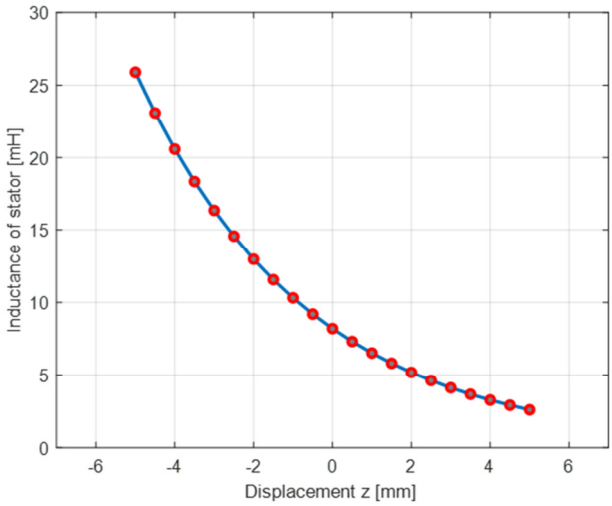

Fig. 3. The results of inductance measurement with respect to the air gap.

B. Experimental Results

In order to validate the proposed control model, an experimental scenario was designed with two cases:

- The sliding mode controller is designed using the initial model without the approximation function $L(z)$.
- The proposed sliding mode controller utilizes the approximation function $L(z)$.

The motor is initialized with a starting position of z = 0.5 mm and an initial speed of zero to test the position stabilization capability. After one second, the motor speed is set to w = 100 rad/s, and after three seconds, a load torque of T = 0.5 Nm is applied. As presented in Figure 4, the absence of the approximation function $L(z)$ in the controller design results in a substantial increase in position instability. These position oscillations subsequently result in variations in inductance, which in turn directly affect the current control loop and, by extension, induce current oscillations. The acceleration of the motor introduces cross-coupling noise to the position control loop, particularly at 1s. This phenomenon can be attributed to the variation in inductance with respect to the position, which in turn causes cross-coupling effects between the speed and position control loops. As shown in Figure 5, the oscillations in position lead to significant fluctuations in speed. The variation in inductance along both the d- and q-axes introduces a delay in the current controller's response when designed assuming constant inductance, thereby intensifying torque oscillations.

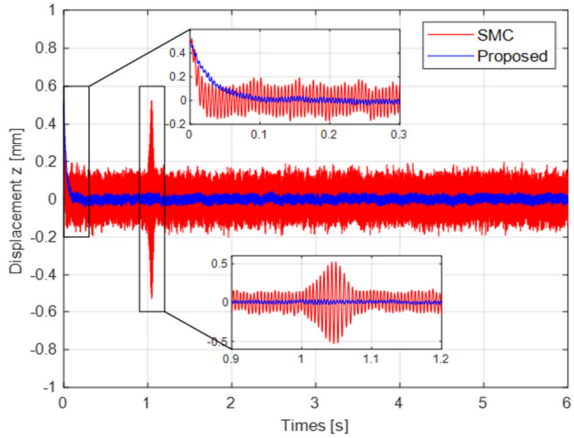

Fig. 4. Experimental results of rotor position.

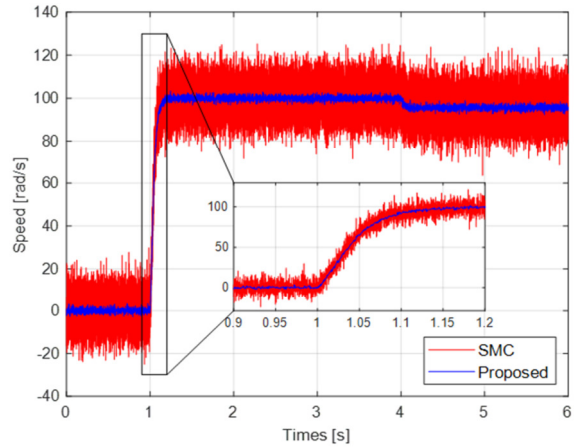

Fig. 5. Experimental results of motor speed.

In contrast, the proposed controller demonstrates the capacity to expeditiously adapt to the inductance variations, hence effectively mitigating the current oscillations. Moreover, Figure 4 reveals that the cross-coupling effect between the speed control loop and the position control loop is negligible, therefore substantiating the efficacy of the proposed control scheme. The experimental results for the currents in stator 1 and stator 2, in scenarios where the variation in inductance is not accounted for, exhibit markedly inferior performance, as portrayed in Figures 6 and 7. Specifically, the current oscillations are notably larger, with fluctuations reaching up to 3A for the i_d current.

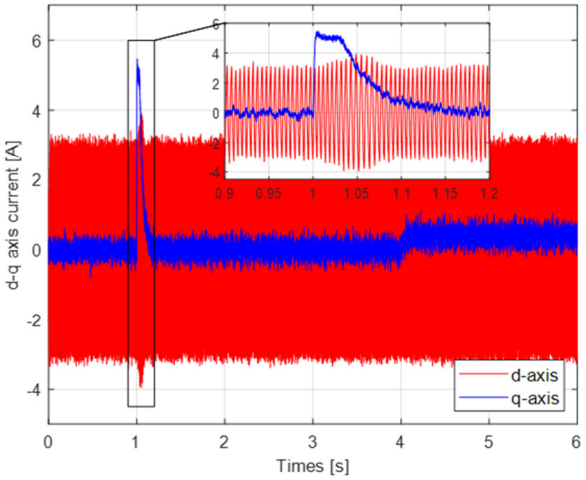

Fig. 6. Experimental results of the i_{dq} current for stator 1 using the SMC without considering the variation of inductance $L(z)$.

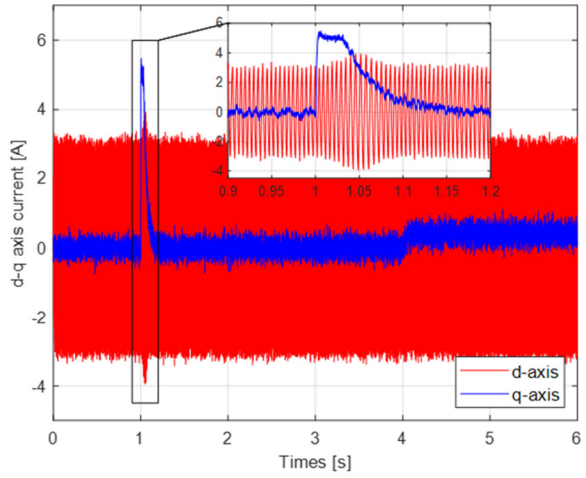

Fig. 7. Experimental results of the i_{dq} current for stator 2 using the sliding mode controller without considering the variation of inductance $L(z)$.

In addition, the oscillation in the i_d current is significantly reduced to approximately 1 A, as shown in Figures 8 and 9. Furthermore, the controller's inherent capacity to adapt to inductance variations is evidenced by the experimental findings, which demonstrate the absence of cross-coupling effects between the speed and position control loops. The

experimental findings have elucidated the impact of the inductance variation on the performance of the controllers. The experimental results indicate that the proposed controller enhances the quality of the response for the position along the z-axis and improves the dynamics of the speed loop.

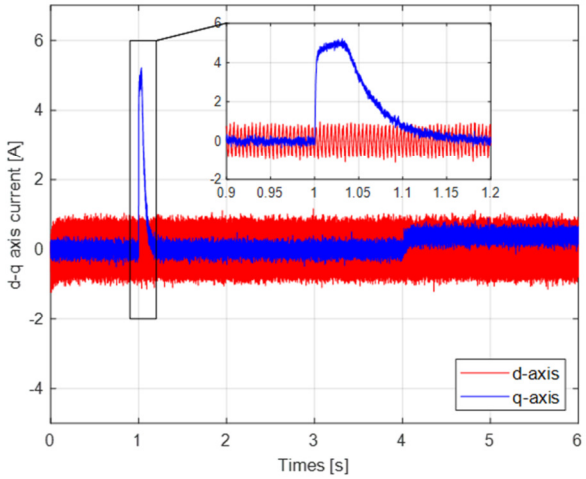

Fig. 8. Experimental results of the i_{dq} current for stator 1 using the SMC considering the variation of inductance $L(z)$.

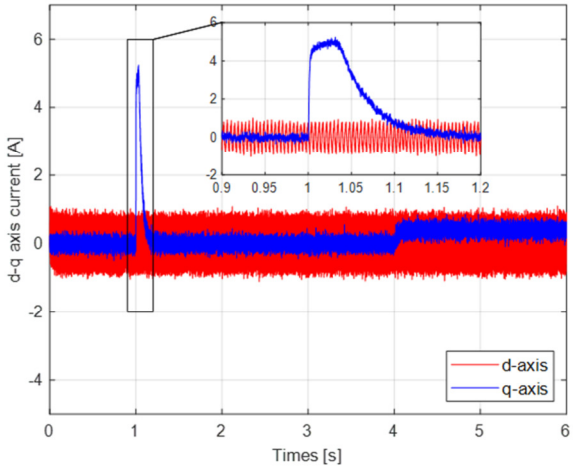

Fig. 9. Experimental results of the i_{dq} current for stator 2 using the SMC with considering the variation of inductance $L(z)$.

V. CONCLUSIONS

Axial-Flux Self-Bearing Motors (AFBMs) are distinguished by their variable inductance during operation. The current paper presents a simplified function to address this issue, with the objective of enhancing the system's overall performance. In addition, a proposal for the design of control systems has been put forth, resulting in the development of a control structure that takes into account the changes in the system's inductance. A motor model has been introduced and its validity has been demonstrated through experimental trials under two conditions: with and without considering the variation in inductance within the controller. The experimental results have demonstrated the efficacy of the proposed control approach by mitigating the coupling effects caused by the inductance variations and stabilizing oscillations. However, the inductance function presented in the paper is based on the experimental results from a specific motor, which poses challenges in the design of a controller that can be universally applied to any arbitrary system. Future research could focus on refining the approximation function to entirely eliminate model discrepancies or on implementing an online identification of these inductances for further optimization.

ACKNOWLEDGMENT

The authors would like to thank Thai Nguyen University of Technology, Vietnam for their facilities and constructive criticism of the manuscript.

REFERENCES

[1] A. Cavagnino, M. Lazzari, F. Profumo, and A. Tenconi, "A comparison between the axial flux and the radial flux structures for PM synchronous motors," *IEEE Transactions on Industry Applications*, vol. 38, no. 6, pp. 1517–1524, Nov. 2002, https://doi.org/10.1109/TIA.2002.805572.

[2] S. Amin, S. Khan, and S. S. Hussain Bukhari, "A Comprehensive Review on Axial Flux Machines and Its Applications," in *2019 2nd International Conference on Computing, Mathematics and Engineering Technologies (iCoMET)*, Sukkur, Pakistan, Jan. 2019, pp. 1–7, https://doi.org/10.1109/ICOMET.2019.8673422.

[3] F. Nishanth, J. Van Verdeghem, and E. L. Severson, "A Review of Axial Flux Permanent Magnet Machine Technology," *IEEE Transactions on Industry Applications*, vol. 59, no. 4, pp. 3920–3933, Jul. 2023, https://doi.org/10.1109/TIA.2023.3258933.

[4] E. Cetin and F. Daldaban, "Reducing Torque Ripples of the Axial Flux PM Motors by Magnet Stepping and Shifting," *Engineering, Technology & Applied Science Research*, vol. 8, no. 1, pp. 2385–2388, Feb. 2018, https://doi.org/10.48084/etasr.1700.

[5] F. Giulii Capponi, G. De Donato, and F. Caricchi, "Recent Advances in Axial-Flux Permanent-Magnet Machine Technology," *IEEE Transactions on Industry Applications*, vol. 48, no. 6, pp. 2190–2205, Nov. 2012, https://doi.org/10.1109/TIA.2012.2226854.

[6] F. C. Mushid and D. G. Dorrell, "Review of axial flux induction motor for automotive applications," in *2017 IEEE Workshop on Electrical Machines Design, Control and Diagnosis (WEMDCD)*, Nottingham, UK, Apr. 2017, pp. 146–151, https://doi.org/10.1109/WEMDCD.2017.7947738.

[7] S. Ueno and Y. Okada, "Characteristics of axial force and rotating torque and their control of permanent magnet type axial gap self-bearing motor," *Electrical Engineering in Japan*, vol. 132, no. 1, pp. 81–91, 2000, https://doi.org/10.1002/(SICI)1520-6416(20000715)132:1<81::AID-EEJ11>3.0.CO;2-P.

[8] Q. D. Nguyen and S. Ueno, "Analysis and Control of Nonsalient Permanent Magnet Axial Gap Self-Bearing Motor," *IEEE Transactions on Industrial Electronics*, vol. 58, no. 7, pp. 2644–2652, Jul. 2011, https://doi.org/10.1109/TIE.2010.2076309.

[9] Q. D. Nguyen and S. Ueno, "Modeling and Control of Salient-Pole Permanent Magnet Axial-Gap Self-Bearing Motor," *IEEE/ASME Transactions on Mechatronics*, vol. 16, no. 3, pp. 518–526, Jun. 2011, https://doi.org/10.1109/TMECH.2010.2045392.

[10] W. Geng and Z. Zhang, "Investigation of a New Ironless-Stator Self-Bearing Axial Flux Permanent Magnet Motor," *IEEE Transactions on Magnetics*, vol. 52, no. 7, pp. 1–4, Jul. 2016, https://doi.org/10.1109/TMAG.2016.2524649.

[11] Q. D. Nguyen and S. Ueno, "Axial position and speed vector control of the inset permanent magnet axial gap type self bearing motor," in *2009 IEEE/ASME International Conference on Advanced Intelligent Mechatronics*, Singapore, Jul. 2009, pp. 130–135, https://doi.org/10.1109/AIM.2009.5230025.

[12] J. Asama, T. K. Tai, and A. Chiba, "Development of Axial-Flux Single-Drive Bearingless Motor With One-Axis Active Positioning," *IEEE*

Transactions on Industry Applications, vol. 57, no. 6, pp. 6792–6800, Nov. 2021, https://doi.org/10.1109/TIA.2021.3096174.

[13] N. P. Quang and J.-A. Dittrich, *Vector Control of Three-Phase AC Machines: System Development in the Practice*. Berlin, Heidelberg: Springer, 2015.

[14] D. Q. Nguyen and S. Ueno, "Sensorless speed control of a permanent magnet type axial gap self-bearing motor using sliding mode observer," in *Robotics and Vision 2008 10th International Conference on Control, Automation*, Hanoi, Vietnam, Dec. 2008, pp. 1600–1605, https://doi.org/10.1109/ICARCV.2008.4795764.

[15] M. Osa, T. Masuzawa, N. Omori, and E. Tatsumi, "Radial position active control of double stator axial gap self-bearing motor for pediatric VAD," *Mechanical Engineering Journal*, vol. 2, no. 4, pp. 15-00105-15–00105, 2015, https://doi.org/10.1299/mej.15-00105.

[16] S. Ueno, K. Nakazawa, and C. Jiang, "Improvement of Stability of an Tilt-Controlling Axial Gap Self-bearing Motor with Single Stator," in *2019 12th Asian Control Conference (ASCC)*, Kitakyushu, Japan, Jun. 2019, pp. 1216–1221.

[17] N. Turk, N. Bulić, and W. Gruber, "Nonlinear Control of a Bearingless Flux-Switching Slice Motor With Combined Winding System," *IEEE/ASME Transactions on Mechatronics*, vol. 25, no. 1, pp. 152–163, Feb. 2020, https://doi.org/10.1109/TMECH.2019.2950871.

[18] V. T. Ha, "Torque Control of an In-Wheel Axial Flux Permanent Magnet Synchronous Motor using a Fuzzy Logic Controller for Electric Vehicles," *Engineering, Technology & Applied Science Research*, vol. 13, no. 2, pp. 10357–10362, Apr. 2023, https://doi.org/10.48084/etasr.5689.

[19] Z. Deng, H. Zhang, X. Wang, and Y. Yan, "Nonlinear Decoupling Control of the Bearingless Induction Motors Based on the Airgap Motor Flux Orientation," *Chinese Journal of Aeronautics*, vol. 15, no. 1, pp. 38–43, Feb. 2002, https://doi.org/10.1016/S1000-9361(11)60128-3.

[20] S. Park, W. Kim, and S.-I. Kim, "A Numerical Prediction Model for Vibration and Noise of Axial Flux Motors," *IEEE Transactions on Industrial Electronics*, vol. 61, no. 10, pp. 5757–5762, Oct. 2014, https://doi.org/10.1109/TIE.2014.2300034.

[21] T.-U. Jung, J.-H. Jang, and C.-S. Park, "A Back-EMF Estimation Error Compensation Method for Accurate Rotor Position Estimation of Surface Mounted Permanent Magnet Synchronous Motors," *Energies*, vol. 10, no. 8, Aug. 2017, Art. no. 1160, https://doi.org/10.3390/en10081160.

[22] B. Song and J. K. Hedrick, *Dynamic Surface Control of Uncertain Nonlinear Systems: An LMI Approach*. London: Springer, 2011.

[23] M. T. Ngo, Q. D. Pham, H. P. Nguyen, and T. L. Nguyen, "Dynamic Surface Control of the Axial-Flux Permanent Magnet Motor with Speed Sensorless Algorithm," in *Advances in Engineering Research and Application*, Cham, Switzerland, 2021, pp. 350–358, https://doi.org/10.1007/978-3-030-64719-3_39.

[24] K. Cherif, A. Sahbani, and K. B. Saad, "Performance Evaluation of PI and Sliding Mode Control for PMSM in Applications for Electric Vehicles," *Engineering, Technology & Applied Science Research*, vol. 14, no. 4, pp. 15464–15470, Aug. 2024, https://doi.org/10.48084/etasr.7172.